The Journal of Experimental Biology 210, 3277-3284
Published by The Company of Biologists 2007
doi:10.1242/jeb.008425

Neural mechanisms underlying target detection in a dragonfly centrifugal neuron

Bart R. H. Geurten[1,*], Karin Nordström[1,†], Jordanna D. H. Sprayberry[2,‡], Douglas M. Bolzon[1] and David C. O'Carroll[1]

[1]*Discipline of Physiology, School of Molecular and Biomedical Science, The University of Adelaide, SA 5005, Australia and* [2]*Department of Zoology, University of Washington, Box 351800, Seattle, WA 98195, USA*

*Present address: Department of Neurobiology, Faculty of Biology, Bielefeld University, Postbox 10 01 31, 33501 Bielefeld, Germany
†Author for correspondence (e-mail: karin.nordstrom@adelaide.edu.au)
‡Present address: Division of Neurobiology, University of Arizona, Tucson, AZ 85721, USA

Accepted 12 July 2007

Summary

Visual identification of targets is an important task for many animals searching for prey or conspecifics. Dragonflies utilize specialized optics in the dorsal acute zone, accompanied by higher-order visual neurons in the lobula complex, and descending neural pathways tuned to the motion of small targets. While recent studies describe the physiology of insect small target motion detector (STMD) neurons, little is known about the mechanisms that underlie their exquisite sensitivity to target motion. Lobula plate tangential cells (LPTCs), a group of neurons in dipteran flies selective for wide-field motion, have been shown to take input from local motion detectors consistent with the classic correlation model developed by Hassenstein and Reichardt in the 1950s. We have tested the hypothesis that similar mechanisms underlie the response of dragonfly STMDs. We show that an anatomically characterized centrifugal STMD neuron (CSTMD1) gives responses that depend strongly on target contrast, a clear prediction of the correlation model. Target stimuli are more complex in spatiotemporal terms than the sinusoidal grating patterns used to study LPTCs, so we used a correlation-based computer model to predict response tuning to velocity and width of moving targets. We show that increasing target width in the direction of travel causes a shift in response tuning to higher velocities, consistent with our model. Finally, we show how the morphology of CSTMD1 allows for impressive spatial interactions when more than one target is present in the visual field.

Key words: target detection, velocity tuning, contrast dependence, spatial interactions, insect vision, elementary motion detection (EMD).

Introduction

Despite the limited acuity provided by the compound eye, many insects detect and pursue small targets, such as prey or conspecifics. This impressive feat is complicated by the need for targets to be visualized against a complex, moving background during pursuit. Among the insects, dragonflies stand out, with sophisticated flight maneuvers where they are seen switching from cruising to high-speed pursuits of prey, with successful catch rates as high as 97% (Olberg et al., 2000).

To aid this task, dragonflies have among the largest compound eyes and smallest interommatidial angles measured in insects, down to as little as 0.24° in the large predator *Aeshna* (see Land, 1997) and around 0.3–0.5° in the dorsally directed acute zone of the smaller corduliid dragonfly *Hemicordulia tau* (Horridge, 1978). The dorsal optical specializations of dragonflies are accompanied by higher-order lobula visual neurons optimized for the detection of small moving targets (O'Carroll, 1993), as well as by descending target neurons providing the information to the flight muscles (Olberg, 1981), with receptive fields in the dorsal part of the visual field. While the optics and the visual pathways for target detection provide a neural basis for the observed behavior, little is known about the input pathways that underlie the impressive sensitivity and selectivity of higher-order small target motion detection (STMD) neurons.

During the past five decades, our understanding of insect vision has improved dramatically. Pathways subserving motion analysis are among the best studied of all neural pathways. One of the earliest models for motion detection, the correlational elementary motion detector (EMD), was described by Hassenstein and Reichardt (Hassenstein and Reichardt, 1956). This model is based on non-linear correlation of the response of one photoreceptor (or other unit) by the delayed response of a neighbor. By subtracting the response of a mirror-image correlator, the EMD gives direction-selective responses to moving features, while ignoring flicker, or static luminance. This model is well supported by physiological and behavioral evidence.

In insects, correlation-type EMDs are believed to form major input to higher levels of motion processing, such as detection of optic flow patterns (see Borst and Haag, 2002). Lobula plate tangential cells (LPTCs), a group of neurons in dipteran flies selective for wide-field motion, have been shown to take input from local motion detectors, consistent with this model

(Egelhaaf et al., 1989; Haag et al., 2004; Hassenstein and Reichardt, 1956). The inherent rejection of non-moving features makes correlation-type EMDs well suited as a preliminary stage in detection and analysis of very small moving targets. STMDs of the hoverfly lobula are often direction selective (Nordström et al., 2006), and some display distinct velocity optima (Nordström and O'Carroll, 2006). While both properties are consistent with correlation-type EMDs, we have not yet directly tested other predictions of this model, as has been used in analysis of LPTCs (Egelhaaf et al., 1989; Haag et al., 2004).

Hoverfly STMDs constitute a large, and to some extent, heterogenous group of small higher-order visual neurons (Nordström et al., 2006). We have yet to encounter a model class of STMD neurons in dipteran flies that provides the robust repeatability of the fly LPTCs for detailed quantitative experimental investigation. However, in the dragonfly *Hemicordulia*, we repeatedly encounter an immediately recognizable STMD neuron with a contralateral receptive field (as compared to the recording site) and large axon that permits recordings of long duration, providing the opportunity for more detailed investigation. In this paper, we describe the basic physiology of this neuron [which we name centrifugal STMD1 (CSTMD1)] to investigate whether dragonfly STMDs utilize correlation-type EMDs as input. We analyzed the response to targets of different contrast and velocity compared with the output of an EMD model elaborated with biologically inspired input filters (spatial and temporal pre-filtering). We provide clear evidence that correlational EMDs (or equivalent processing) are on the input pathway to STMDs. We finally show that complex spatial interactions permitted by the complex dendritic tree of CSTMD1 might be involved in the exquisite tuning of STMDs to small targets.

Materials and methods

Experimental setup

Wild-caught dragonflies (*Hemicordulia tau* Selsius and *Hemicordulia australiae* Rambur) were immobilized with wax, and the head was tilted forward to gain access to the posterior head surface. A small hole was cut over the left lobula complex, leaving the perineural sheath intact. Neurons were recorded intracellularly using aluminum silicate micropipettes pulled on a Sutter Instruments P-97 puller and filled with 2 mol l^{-1} KCl. Electrodes had a typical tip resistance of 120 MΩ. The dragonfly was mounted in front of a 48 cm RGB CRT visual display with a high refresh rate (200 Hz) and a mean luminance of 150 Cd m^{-2}. The dragonflies were mounted in front of the display at a distance of 15–20 cm. They were aligned with the monitor using the planar back surface of the head as a morphological landmark, and the animal's equator was assumed to be 90° perpendicular to this. The animal's midline was used to determine the vertical meridian. This was used in later analyses to determine receptive field size and location, and stimuli size and velocity.

Visual stimuli were presented using VisionEgg software (http://www.visionegg.org). The display subtended approximately 100×75° of the animal's visual field of view, with a resolution of 640×480 pixels, permitting targets down to 0.15° to be presented. Data were digitized at 5 kHz using a 16-bit A/D converter (National Instruments, Austin, TX, USA) and analyzed both on-line and off-line with Matlab software (The Mathworks Inc., Natick, MA, USA). Data in Fig. 5 show a recording using the Picassso Image Synthesizer on a Tectronix 608 XYZ display.

Neuron characterization

We recorded intracellularly from neurons in the left lobula. Receptive fields and directionality of neurons that responded to small targets were determined using a series of 21 horizontal and vertical scans with a high-contrast 0.8×0.8° target moving at 50 deg. s^{-1} across the bright CRT display.

Subsequently, targets were presented moving in a single path through the centre of the receptive field. We defined neurons as STMDs using similar criteria to our recent studies (Barnett et al., 2007; Nordström et al., 2006). Target specificity was determined using a series of bars of variable height and the width fixed at 0.6° drifting at 26 deg. s^{-1}. We recorded from over 50 neurons identified as STMDs.

To estimate velocity tuning we drifted a 0.8×0.8° square and an 8° wide by 0.8° high black target across the centre of the receptive field at velocities ranging between 6 deg. s^{-1} and 600 deg. s^{-1}. The targets were presented moving horizontally in the preferred direction and included a minimum 3 s rest between presentations.

We altered target contrast by increasing the luminance of the target (I_{target}) against the bright background of the display ($I_{background}$), quantified using the Michelson definition:

$$(I_{background} - I_{target}) / (I_{background} + I_{target}) . \quad (1)$$

To analyze the presence of spatial inhibition within and outside the receptive field, we presented two targets traversing the receptive field with varying horizontal separation. The two targets scanned the monitor at 40 deg. s^{-1} along the same horizontal path. We varied the horizontal distance between the two targets from 0.6° (creating one elongated target) to 40° as measured from center to center of the two targets.

Data analysis

Analysis of spiking responses was carried out off-line in Matlab by band-pass filtering the digitized response and then detecting spikes using an algorithm that makes use of both edge and relative magnitude (level) cues. Receptive fields were obtained from the horizontal scans using the methods we developed previously for fly STMDs (Nordström et al., 2006). The peri-stimulus time histogram was divided into 21 bins, corresponding to 5° intervals on the two-dimensional display. We further analyzed the local preferred direction using a method analogous to that used previously for fly LPTCs (Krapp and Hengstenberg, 1997) and dragonfly descending neurons (Frye and Olberg, 1995). The response to four directions of motion at each point in the receptive field was fitted in a least-squares manner with a sinusoid of variable phase, amplitude and offset but a fixed period of 360°. We then used the phase of the fitted function to infer the local preferred direction, plotted as the orientation of a local vector, and the relative amplitude (after normalizing for the overall maximum response of the neuron) as the length of the local vector.

For all other experiments we measured the spike rate during the time the target traversed the receptive field, as a function of

the varied parameter. For each experiment we performed 1–3 repeats in each animal. Where more than one repeat was performed, we calculated the mean of the repeats for further analysis. Given *N*-values thus represent the number of animals subjected to each particular test.

Morphology

To identify recorded neurons, we backfilled micropipettes with 4% Lucifer Yellow in 0.1 mol l^{-1} LiCl. The dye was injected by passing a hyperpolarizing current (0.2–2 nA, depending on the amount of current individual electrodes would pass without blockage) for 1–10 min. Following electrophysiology, the brain was dissected out of the head capsule, fixed in 4% paraformaldehyde (in 0.1 mol l^{-1} phosphate buffer), dehydrated through an ethanol series and cleared in methyl salicylate. A *z*-series of photographs from the whole-mount was used to reconstruct the morphology of the neuron.

EMD modeling

To predict the effect of altering target size (width in the same direction as travel) on velocity tuning we simulated a one-dimensional array of elementary motion detectors (EMDs) in a 360° ring configuration using Matlab software. The inputs to the model were dark targets (luminance 0) animated against a bright background (luminance 1), as in the biological experiments. Photoreceptor input was spatially filtered (Gaussian blur) and sampled to yield an interommatidial angle of 0.56° and an acceptance angle of 0.78° based on optical data for *Hemicordulia* (Horridge, 1978) and yielding a ring of 640 EMDs. To account for at least some minimal (linear) high-pass temporal filtering likely in the insect visual system, this signal was then convolved with a kernel based on that obtained through white-noise analysis of fly monopolar cells (James, 1990) and fitted with a double log-normal function of the form:

$$h(t) = a_1 \exp\{-[\log(t/tp_1)]^2/2{s_1}^2\} + a_2 \exp\{-[\log(t/tp_2)]^2/2{s_2}^2\}\,, \quad (2)$$

where $h(t)$ is the filter impulse response at time t, a denotes the amplitude of the response (a_1=1.06; a_2=–0.167), tp denotes the time-to-peak (tp_1=10.1 ms; tp_2=17.5 ms) and s denotes the sigma shape of the response (s_1=0.197; s_2=0.345). This luminance signal was then fed into the one-dimensional EMD array incorporating a temporal delay of 35 ms (modeled as a 1st-order low-pass filter). The undelayed signal from one arm of the EMD was multiplied by the delayed signal from the neighboring arm. This process was repeated in a mirror symmetrical fashion and the two outputs subtracted from each other (Hassenstein and Reichardt, 1956). The simulation was run at a resolution of 1000 samples per second and 100 samples per degree of visual space. The ring configuration of the EMD array (and the fact that the target is thus always within the 'receptive field' of the EMD array) allowed us to conveniently estimate a response (the linear sum of responses of all EMDs at any instant in time) equivalent to the steady-state response of the system to a sinusoidal grating stimulus, even though the response of any single EMD is a complex, transient phenomenon. This allowed us to explore the response as a function of the speed and spatial dimensions.

Results

Basic characterization of responses

We recorded intracellularly from 40 *Hemicordulia (H. tau* and *H. australiae*) dragonflies. In order to confirm quantitatively that penetrated neurons were STMDs, we recorded responses to targets of different heights and the width fixed at 0.6–0.8°. The size tuning of the recorded STMDs followed that previously described (then labeled 'small target-sensitive') (see O'Carroll, 1993) with a peak response around 1–2° and little response to bars over 10° high, or to widefield stimuli such as gratings (Fig. 1A and Fig. 2).

The diversity of dragonfly STMDs might easily be as great as that of hoverflies (Nordström et al., 2006). Based on the above criteria, we identified 50 neurons as STMDs, exhibiting a wide variety of receptive fields and other properties [ranging from STMDs with very small receptive fields as described in the hoverfly (Barnett et al., 2007) to neurons with massive homolateral, or even heterolateral, receptive fields]. We repeatedly encountered a neuron that provided stable recordings (up to 4 h in some cases) and thus provided a good basis for more detailed study. This neuron has a moderate-sized (~30° width) contralateral (as compared to recording site), dorsal receptive field (Fig. 1B). The neuron gives very characteristic large (up to 100 mV), fast (duration <3 ms), bi-phasic action potentials. In the healthiest recordings, the STMD shows little spontaneous activity, but many penetrations from the same neuron (confirmed by successful dye injection on seven occasions) yield characteristic regular spontaneous firing at approximately 20 Hz.

Neuroanatomy of CSTMD1

Dye fills of the STMD (black in Fig. 1C) reveal a large axon traversing the protocerebrum from the right hemisphere (we recorded intracellularly from the left hemisphere). We have thus given it the anatomically descriptive name CSTMD1 (centrifugal small target motion detector 1). CSTMD1 shows a mass of dense arborizations, with a heavily beaded appearance across the entire distal left lobula (inset I, Fig. 1C). There are two additional arborizations in the ventro-lateral protocerebrum on both sides (insets II and III, Fig. 1C). The soma is located adjacent to the arborizations in the right midbrain. Combined with the sparse, unbeaded (spiny) appearance of dendrites in this region (inset III, Fig. 1C), these observations suggest that this is the input region. This is further confirmed by the physiologically recorded receptive field with excitation confined to the right visual field (Fig. 1B). The midbrain dendrites in the left hemisphere have a beaded appearance, suggesting output synapses (inset II, Fig. 1C). Interestingly, if we overlay a mirror image reconstruction (red in Fig. 1C), the two midbrain arborizations are co-located, suggesting the possibility that this neuron makes synaptic contact with its contralateral counterpart.

We have based our definition of neurons as CSTMD1 on the physiological and anatomical characteristics described in Fig. 1. Even though there might be a small chance that the CSTMD1 'class' could include additional neurons with similar physiological and anatomical characteristics, such redundancy in a small insect brain is unlikely.

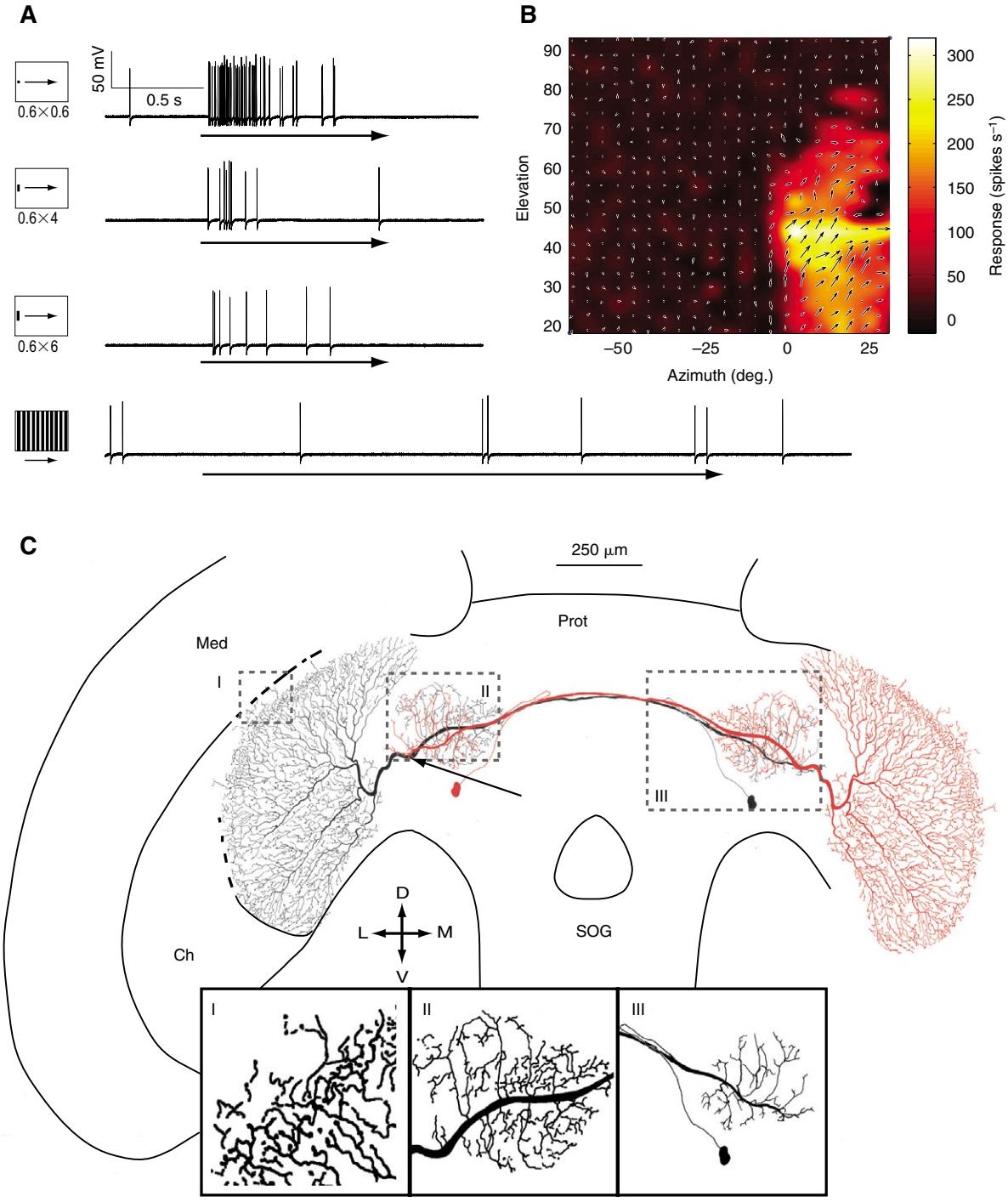

Fig. 1. Characterization of CSTMD1. (A) Intracellular responses to targets of different sizes illustrate the extreme size selectivity of CSTMD1. While a 0.6×0.6° high-contrast target traversing the receptive field evokes a strong response (top trace), larger targets elicit lower spike frequencies (middle traces), and full screen gratings (bottom trace) give no response above spontaneous firing rates. The targets scanned the center of the receptive field at 26 deg. s^{-1}, as indicated by arrows under each trace. (B) A physiologically recorded (from the left hemisphere) CSTMD1 receptive field shows excitation in the opposite hemisphere only. The false color plot was generated by scanning the entire monitor horizontally with a high-contrast 0.8×0.8° target 21 equidistant locations at 50 deg. s^{-1}. Arrows indicate the strength of the directionality at each location as constructed by drifting targets in four directions across the stimulus display (see Materials and methods). Elevation values are positive above the equator, and azimuths negative to the left of the midline. (C) A reconstructed Lucifer Yellow fill of CSTMD1 shows massive arborizations (black) in the left hemisphere (recording side). As the soma is located in the opposite hemisphere, and the dendrites of this hemisphere are not beaded (inset III) unlike the arborizations on the left side (insets I and II), the right side most probably provides the input. A displayed mirror image projection of the neuron (red) shows how output arborizations (II) from one hemisphere co-localize with input dendrites from the other hemisphere (III), thus providing the opportunity for synaptic control of responses. Arrow indicates the recording site. Med, medulla; Ch, inner optic chiasm; Prot, protocerebrum; SOG, sub-oesophageal ganglion; L, lateral; D, dorsal; M, medial; V, ventral.

Contrast dependency

The EMD model is based on non-linear correlation of the response of one photoreceptor by the delayed response of a neighbor (Hassenstein and Reichardt, 1956). This non-linearity (usually modeled as multiplication) leads to a characteristic dependence on pattern contrast, as observed in numerous recordings from LPTCs (Egelhaaf et al., 1989; Haag et al., 2004; Harris et al., 2000). To test for a similar effect in CSTMD1, we scanned the center of the receptive field with 0.6×0.6° targets of varying contrast moving at 26 deg. s^{-1} (Fig. 3). Our data show a strong dependence on the contrast of the target. This does not saturate as obviously as in LPTCs (Harris et al., 2000), possibly reflecting the smaller-than-optimal target size (which may not reach the same effective contrast as is possible with a wide-field grating), but the contrast response function has an overall similar form. Our data thus support a similar mechanism for the underlying motion detectors to those in the LPTCs.

Direction selectivity

Another hallmark of the correlation model is the inherent direction selectivity of the response. While our previous work (Barnett et al., 2007; Nordström et al., 2006) has revealed both directional and non-directional STMD neurons, the latter could still comprise the summed output of EMDs with different preferred directions. Fig. 2 shows that responses of CSTMD1 to all target sizes were stronger for targets moving from the midline to the back of the eye. By constructing local vectors representing the local direction selectivity, the receptive field map (Fig. 1B) suggests that local optima are for targets moving up and away from the frontal visual view point. However, as all scans were performed in the same order, with the preferred direction (right and up) followed by the less preferred (left and down), we cannot rule out habituation to have an effect on this response.

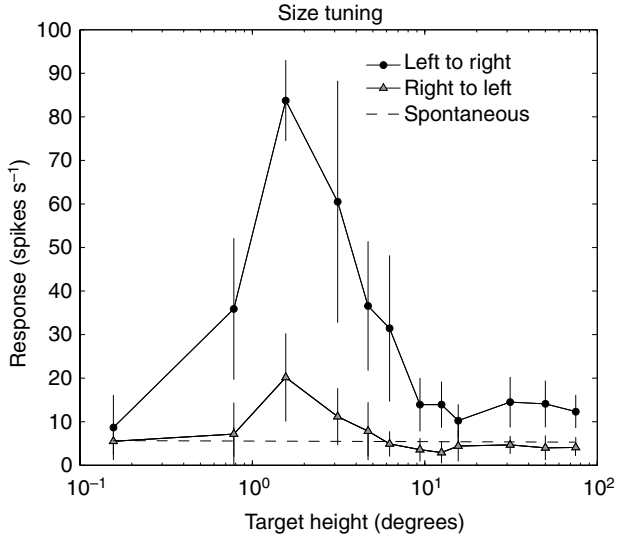

Fig. 2. Size tuning of the dragonfly CSTMD1. Responses to targets of different heights are shown averaged for the time the target traversed the receptive field from left to right (black circles) followed by scans from right to left (gray triangles). The target width was fixed at 0.8° and the targets scanned the receptive field at 50 deg. s^{-1}. The dashed line indicates pre-stimulus spontaneous firing rates. Error bars denote standard error of the mean (*N*=3).

Effect of target size on velocity tuning

The velocity tuning of an EMD array is influenced by the spatial statistics of the image (Buchner, 1984). While this is easy to confirm in dipteran LPTCs using sine-wave gratings, which have all of their power at a single spatial frequency, STMDs only respond to discrete targets, for which the spatial frequency is less easily defined. We used a computer model to predict the effect of target size on the velocity tuning of STMDs for discrete targets of different width (0.8° and 8° wide). The non-linear interaction between the leading and trailing edges of the small target leads to a complex tri-phasic response at low velocities (i.e. transiently inhibited even during preferred direction motion), becoming biphasic (and briefer) as speed increases (Fig. 4A). For a wider target, the response form is different, as the leading and trailing edge responses are separated further at low velocities (Fig. 4B). Whilst the specific shape of these transient responses depends on the temporal filters modeled in the system (data not shown), all such models show shift in the overall velocity optimum (i.e. the peak in the instantaneous sum of all EMDs) from low to high velocities for the wider target (Fig. 4C).

To test whether this prediction holds for dragonfly STMDs, we scanned the center of the receptive field with high-contrast targets of the same two sizes (0.8° and 8° wide, by 0.8° high) moving at velocities between 6 deg. s^{-1} and 600 deg. s^{-1}. The neurons show a maximum response around 60 deg. s^{-1} to the smaller target used (Fig. 4D). As predicted by the mean model output (Fig. 4C), the peak has shifted to a higher velocity (~190 deg. s^{-1}) for wider targets. The maximum response is also lower, reflecting the specificity of STMDs for small targets (Fig. 2).

Further evidence for the specificity of the effect of target spatial dimensions on velocity tuning comes from an

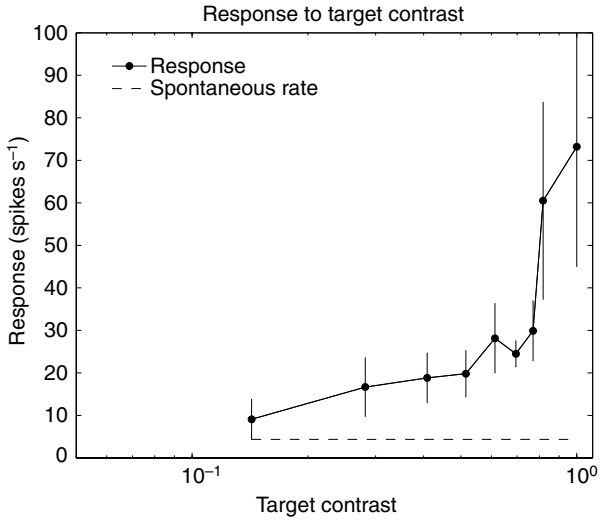

Fig. 3. The response of CSTMD1 to target contrast. Responses to targets (0.6×0.6°) of different contrast are averaged for the time during which they traversed the center of the receptive field at 26 deg. s^{-1}. Error bars denote standard error of the mean (*N*=4).

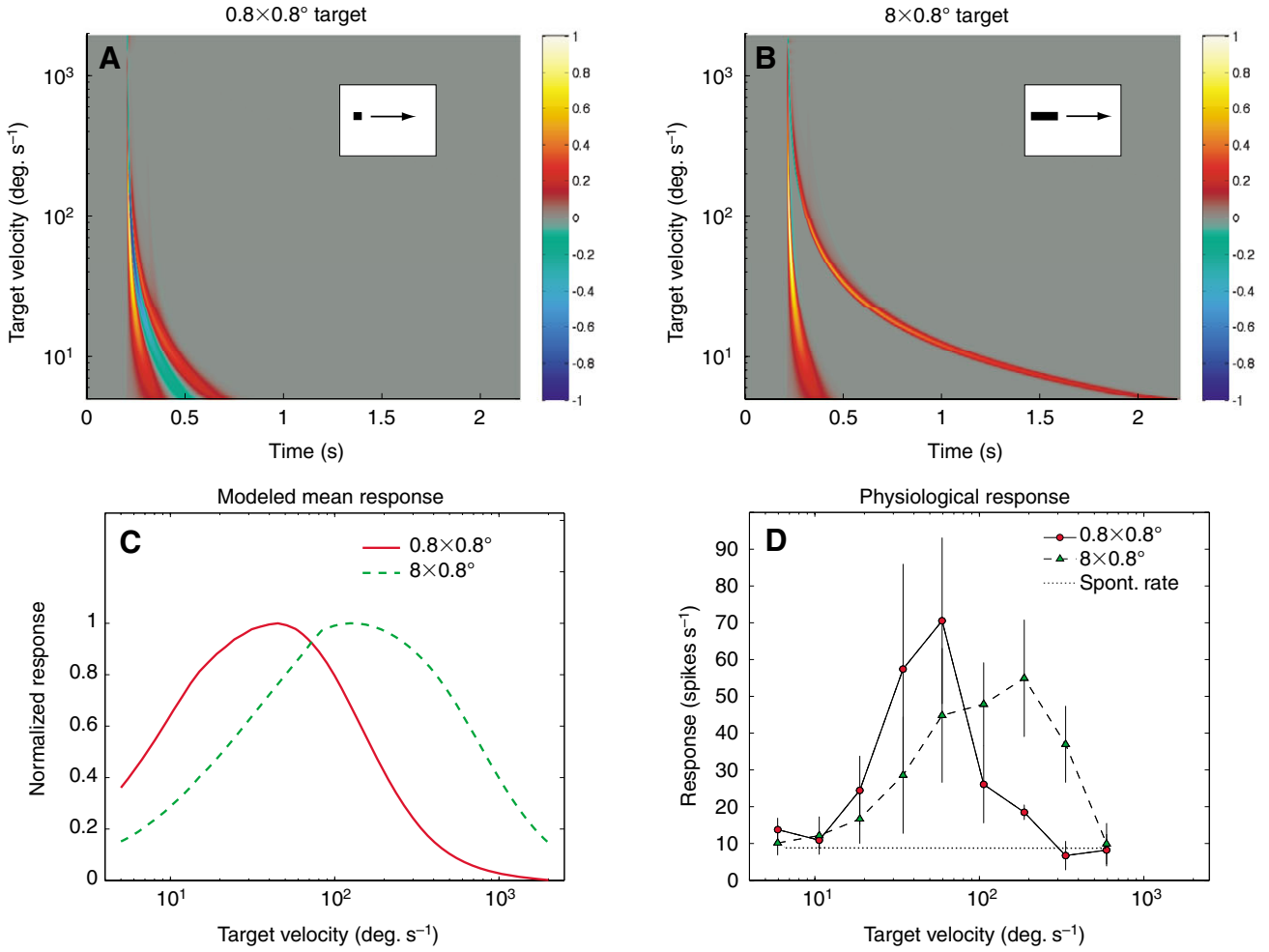

Fig. 4. Velocity tuning to differently sized targets. (A) The false color plot shows the normalized modeled response to a small high-contrast target (0.8°, see inset) traversing a one-dimensional elementary motion detector (EMD) array at velocities between 5 and 2000 deg. s^{-1}. (B) The false color plot shows the normalized modeled response to a wide high-contrast target (8°, see inset) traversing a one-dimensional EMD array. (C) The mean model output shows the response of the EMD array to targets of two widths (0.8° in red line and 8° wide in green line). (D) The graph shows the physiologically recorded response of dragonfly STMDs to target velocity as black targets traversed the center of the receptive field. Two sizes were used: 0.8×0.8° (red circles, solid line) and 8° wide × 0.8° high (green triangles, broken line). Error bars denote standard error of the mean (*N*=4, two of which were CSTMD1s).

experiment that we have thus far replicated for a single CSTMD1 neuron (Fig. 5). Velocity tuning for three different targets, oriented parallel to the direction of travel, shows a shift to higher velocity as in Fig. 4D. However, if we rotate the orientation 90° (i.e. orthogonal to the direction of motion), the velocity tuning for the three targets all peak at similar values, being simply inhibited as target length is increased (Fig. 5B). Overall, the results of these experiments show a dependence of velocity tuning on spatial structure consistent with the EMD model, despite the evidence for spatial inhibitory mechanisms that tune the system to small targets.

Spatial interactions within and outside the receptive field

While the above experiments suggest strongly that a correlation-type EMD or equivalent mechanism is operating at early stages in the STMD pathway, there is nothing in such a model (including our computational implementation of it) to explain the sharp tuning of these neurons to target length (i.e. orthogonal to the direction of motion), as shown in earlier work (Barnett et al., 2007; Nordström et al., 2006) or in Fig. 2 for CSTMD1. While we have previously proposed models to explain such tuning based on spatial inhibitory interactions within the receptive field (Barnett et al., 2007; Nordström et al., 2006), it is more complex to consider the effects of such inhibitory mechanisms *along* the direction of travel, because of the addition of the interactions in the time domain (as evident from the effect of target width on velocity tuning in Fig. 4D and Fig. 5A). To overcome this limitation, we instead examined the inhibitory effect of a second target of equal size, moving along the same track but at a varying horizontal distance (Fig. 6). When the two targets are separated by large angles, the response to each passing into the contralateral receptive field is distinct (Fig. 6A). As the target separation is decreased, there is clear evidence for an interaction between the responses to the two targets, with spike rates never reaching that observed for single targets (see Fig. 2). By a target separation of 5°, the response is

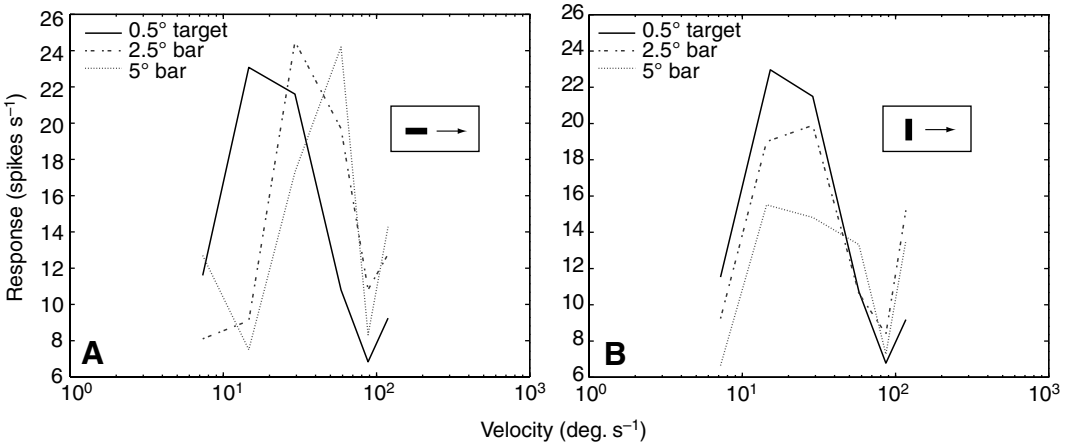

Fig. 5. Velocity tuning to targets of different orientation. (A) The response of a single CSTMD1 to targets oriented along the direction of travel (inset) shows a shift in velocity tuning to higher velocities with wider targets. (B) When the targets are oriented perpendicular to the direction of travel (inset) they all show the same velocity optimum, but the response is reduced for larger targets.

largely abolished in the individual trace (Fig. 6C, left column) and it is also significantly reduced over three trials in the same neuron (Fig. 6C, histogram in right column). Smaller separations see a partial recovery of response towards control levels, as the two targets effectively fuse to become one (Fig. 6D,E).

With this experimental design it is difficult to preclude the possibility that the 'inhibitory' effect arises from habituation or some other adaptive process, since the second target passes across the same local motion detectors as the first, with a short delay (~120 ms for a separation of 5°). However, this is unlikely to explain the depression of the response to the first target for a separation of 15° (Fig. 6B), where the second target is still in the left visual field (see Fig. 1B) when the first target crosses the visual midline and into the excitatory receptive field of CSTMD1. Further work is required, using other controls to preclude habituation effects to fully explore the inhibitory mechanisms revealed by this stimulus. However, given

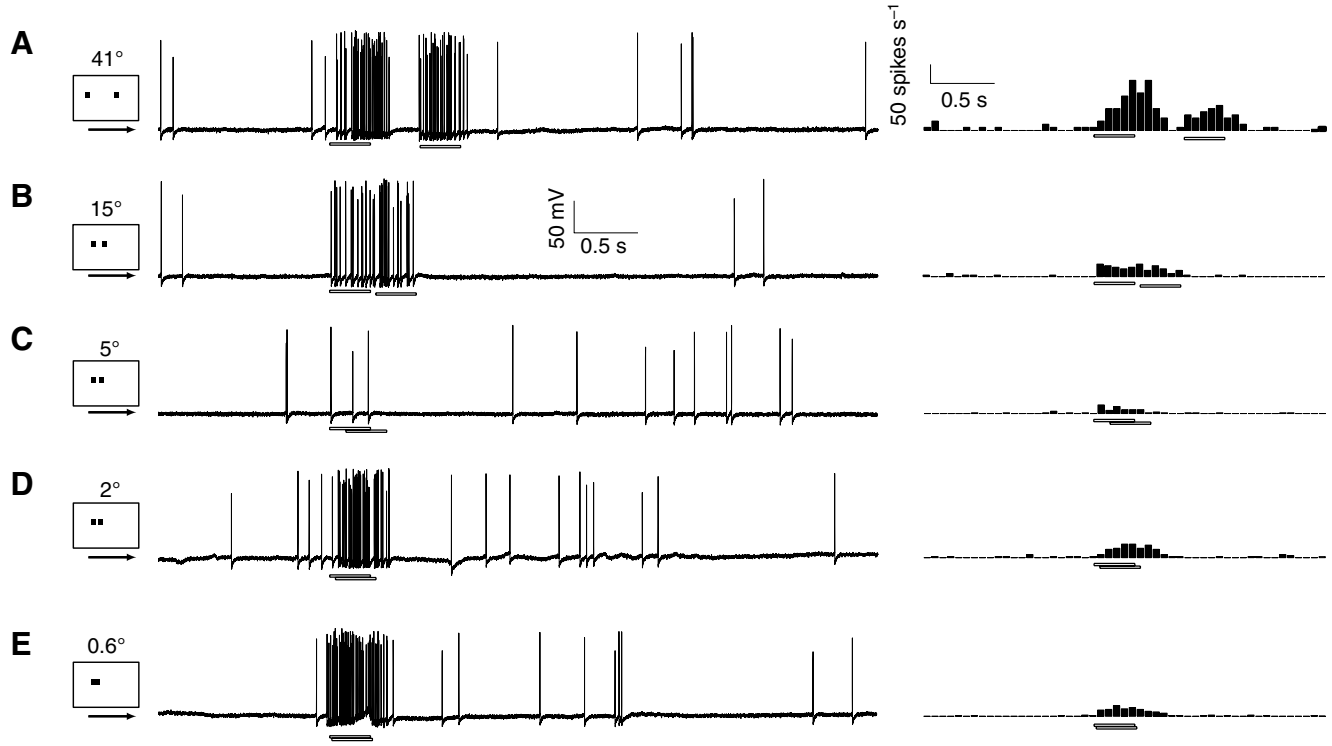

Fig. 6. Spatial interactions between two moving targets. (A) The data trace (on the left) shows the response to two targets traversing the center of the receptive field (as indicated by horizontal bars under the trace) of CSTMD1 at 41 deg. s^{-1}. The two 0.6×0.6° high-contrast targets were separated by 41° (measured from center to center). The histogram on the right shows the mean of three repeats from the same neuron, divided into 50 ms bins. (B) The response of CSTMD1 to two targets separated by 15°. (C) The response to two targets separated by 5°. (D) The response to two targets separated by 2°. (E) The response to two targets separated by 0.6° (in effect creating one elongated target).

interommatidial angles of 0.56° (Horridge, 1978), it is interesting to speculate that the strongest inhibitory interactions occur *within* the receptive field and at separations equivalent to 10 ommatidia. The suppression of responses by targets in the visual field of the opposite eye might result from a second mechanism, mediated by the heterolateral axon in CSTMD1. Given the observation that these neurons bear a likely output arborization corresponding to the inputs of their contralateral counterparts (Fig. 1C), it is plausible to suggest that these neurons form a reciprocal inhibitory pair.

Discussion

As in STMDs of dipteran flies (Barnett et al., 2007; Gilbert and Strausfeld, 1991), the receptive fields of target-sensitive neurons of the dragonfly ventral nerve cord coincide with the location of the dorsal acute zone (Olberg, 1981). It has more recently been shown that dragonflies fix the location of the prey in this dorsal acute zone during pursuit (Olberg et al., 2007). These behavioral investigations showed dragonflies to give a peak preference for small targets of 0.2–0.5° of the visual field (Olberg et al., 2005) while CSTMD1 described here shows a peak response to slightly larger targets (Fig. 2). Direct or indirect CSTMD1 output to descending pathways remains to be shown. However, CSTMD1 could still be involved in prey detection and capture by modulating the response of other STMDs.

The anatomy of hoverfly STMDs (Barnett et al., 2007; Nordström et al., 2006) and of blowfly target neurons (Strausfeld, 1991) shows relatively constrained arborizations and small axons. Compared to these, the dragonfly CSTMD1 is huge (Fig. 1C). In dipterans, neurons of equal size are usually involved in optic flow analysis, necessitating input from a large part of the visual field. The receptive field of CSTMD1 is also larger than its dipteran counterparts (Fig. 1B). The huge output arborizations (Fig. 1C) would furthermore provide opportunities for synaptic feedback to other lobula neurons, as well as to its contralateral partner. This latter case might provide an opportunity for focusing on one target in a swarm of prey – thus optimizing successful catch rates – as indicated by the intriguing spatial interactions shown in Fig. 6.

We thank the Manager of the Botanic Gardens for allowing insect collection. We also thank Dr Russell Brinkworth for the ongoing development of our data acquisition software, and Dr Patrick Shoemaker for ongoing discussions. Prof. Martin Egelhaaf, Dr Rafael Kurtz and Paul Barnett provided helpful feedback on earlier versions of this manuscript. This work was funded by the Swedish Research Council (Post Doc grant to K.N.), the German Study Foundation (graduation grant to B.R.G.) and the US Air Force Office of Scientific Research (FA 9550-04-1-0294).

References

Barnett, P. D., Nordström, K. and O'Carroll, D. C. (2007). Retinotopic organization of small-field-target-detecting neurons in the insect visual system. *Curr. Biol.* **17**, 569-578.

Borst, A. and Haag, J. (2002). Neural networks in the cockpit of the fly. *J. Comp. Physiol. A* **188**, 419-437.

Buchner, E. (1984). Behavioral analysis of spatial vision in insects. In *Photoreception and Vision in Invertebrates* (ed. M. Ali), pp. 561-621. New York: Plenum Press.

Egelhaaf, M., Borst, A. and Reichardt, W. (1989). Computational structure of a biological motion-detection system as revealed by local detector analysis in the fly's nervous system. *J. Opt. Soc. Am. A Opt. Image Sci. Vis.* **6**, 1070-1087.

Frye, M. A. and Olberg, R. M. (1995). Visual receptive field properties of feature detecting neurons in the dragonfly. *J. Comp. Physiol. A* **177**, 569-576.

Gilbert, C. and Strausfeld, N. J. (1991). The functional organization of male-specific visual neurons in flies. *J. Comp. Physiol. A* **169**, 395-411.

Haag, J., Denk, W. and Borst, A. (2004). Fly motion vision is based on Reichardt detectors regardless of the signal-to-noise ratio. *Proc. Natl. Acad. Sci. USA* **101**, 16333-16338.

Harris, R. A., O'Carroll, D. C. and Laughlin, S. B. (2000). Contrast gain reduction in fly motion adaptation. *Neuron* **28**, 595-606.

Hassenstein, B. and Reichardt, W. (1956). Systemtheoretische Analyse der Zeit, Reihenfolgen und Vorzeichenauswertung Bei der Bewegungsperzeption des Rüsselkafers *Chlorophanus*. *Z. Naturforsch.* **11**, 513-524.

Horridge, G. A. (1978). The separation of visual axes in apposition compound eyes. *Philos. Trans. R. Soc. Lond. B Biol. Sci.* **285**, 1-59.

James, A. C. (1990). White-noise studies in the fly lamina. PhD thesis, Australian National University, Canberra, Australia.

Krapp, H. G. and Hengstenberg, R. (1997). A fast stimulus procedure to determine local receptive field properties of motion-sensitive visual interneurons. *Vision Res.* **37**, 225-234.

Land, M. F. (1997). Visual acuity in insects. *Annu. Rev. Entomol.* **42**, 147-177.

Nordström, K. and O'Carroll, D. C. (2006). Small object detection neurons in female hoverflies. *Proc. R. Soc. Lond. B Biol. Sci.* **273**, 1211-1216.

Nordström, K., Barnett, P. D. and O'Carroll, D. C. (2006). Insect detection of small targets moving in visual clutter. *PLoS Biol.* **4**, 378-386.

O'Carroll, D. (1993). Feature-detecting neurons in dragonflies. *Nature* **362**, 541-543.

Olberg, R. M. (1981). Object- and self-movement detectors in the ventral nerve cord of the dragonfly. *J. Comp. Physiol. A* **141**, 327-334.

Olberg, R. M., Worthington, A. H. and Venator, K. R. (2000). Prey pursuit and interception in dragonflies. *J. Comp. Physiol. A* **186**, 155-162.

Olberg, R. M., Worthington, A. H., Fox, J. L., Bessette, C. E. and Loosemore, M. P. (2005). Prey size selection and distance estimation in foraging adult dragonflies. *J. Comp. Physiol. A* **191**, 791-797.

Olberg, R. M., Seaman, R. C., Coats, M. I. and Henry, A. F. (2007). Eye movements and target fixation during dragonfly prey-interception flights. *J. Comp. Physiol. A* **193**, doi: 10.1007/s00359-007-0223-0.

Strausfeld, N. J. (1991). Structural organization of male-specific visual neurons in calliphorid optic lobes. *J. Comp. Physiol. A* **169**, 379-393.